RSC Advances

PAPER

View Article Online
View Journal | View Issue

Cite this: *RSC Adv.*, 2014, **4**, 16985

Promoting effects of ceria on the catalytic performance of gold supported on TiO_2 for low-temperature CO oxidation

Jun Yu,[ab] Guisheng Wu,[a] Guanzhong Lu,*[ab] Dongsen Mao[a] and Yun Guo[b]

Received 17th January 2014
Accepted 17th February 2014

DOI: 10.1039/c3ra47226d

www.rsc.org/advances

The La or Ce-doped TiO_2 prepared by a sol–gel method was used as the support, and supported gold catalysts for CO oxidation were prepared by the deposition–precipitation method. These Au catalysts were characterized by N_2 adsorption–desorption, ICP, XRD, TEM, H_2-TPR, and *in situ* FT-IR. It was found that doping Ce or La in the TiO_2 support obviously improved the catalytic activity and stability of the Au catalysts for CO oxidation. The promoting effect of CeO_2 on its catalytic activity is much larger than La_2O_3. The presence of Ce not only increases the surface area of TiO_2 and restrains the growth of TiO_2 crystallites, but it also enhances the microstrain of TiO_2 and reinforces the interaction between TiO_2 and Au. As a result of the redox efficiency of CeO_2, the synergistic interaction between the Au particles and support, the activity of the active sites and the reactivity of the surface oxygen species, are remarkably improved. Moreover, the effortless decomposition of carbonates and the quick recovery of oxygen vacancies on the Au/Ce–TiO_2 surface might be responsible for the high stability of the Au catalyst, compared with the Au/TiO_2 catalyst.

1. Introduction

Gold as a catalytic component has attracted little attention during the development of heterogeneous catalysts over the past 50 years. This is because it is typically less catalytically active than other platinum group metals. However, when gold nano-particles are highly dispersed on different supports, they exhibit surprisingly high activity for several reactions, such as methanol synthesis, water gas shift and automotive exhaust control.[1–6] CO oxidation can even occur at temperatures below room temperature with nano-Au supported on TiO_2 as the catalyst.[7–10] Therefore, a large number of investigations were employed to develop nano-gold catalysts, and to clarify the key factors that influence the catalytic activity of Au/TiO_2 for CO oxidation at low temperatures.[11–16]

The results of this research show that the catalytic activity of Au/TiO_2 depends on the particle size of Au, the physicochemical properties of the support and the interaction between Au particles and the support. However the issue of the active sites remains a matter of debate: some authors suggest that metallic gold is more active,[17–19] and others argue that oxidized gold is more active.[20–22] Up to now, the deactivation of nano-Au catalysts is still a great and insurmountable obstacle for their commercial application. Some authors have attributed this to sintering of the gold particles, while other authors thought that the interaction between gold and TiO_2 plays a vital role in maintaining the high activity of Au/TiO_2.[14,16,23]

In order to further improve the catalytic activity, and especially the stability of Au/TiO_2 catalysts, the surface modification of the TiO_2 support was studied. Ma *et al.* studied the performance of Au/TiO_2 doped with rare earth (RE) ions, and found that after the addition of RE ions an excellent activity was retained at ambient temperatures, and the dispersion of Au was enhanced.[24] Due to the high oxygen storage capacity and redox of ceria, the presence of ceria in Au/CeO_2/SiO_2 can affect the state and structure of the support and the interaction between gold and the support.[25] Idakiev *et al.* reported that ceria-modified TiO_2 is of much interest as a potential support for the gold-based catalyst for the water-gas shift reaction.[26] Recently, Li *et al.* reported that CeO_2 dominated Au/CeO_2–TiO_2 nanorods are able to promote oxygen migration and gold dispersion, resulting in an evident increase in their catalytic activity for CO oxidation.[27] However, the promoting effect of RE additives proposed by most of the researchers was attributed to their good thermal stability and high spontaneous dispersion.[24–28] The role of the RE additives in the nature of the active sites is still unclear and needs to be investigated. Moreover, the comparison of the stability of the gold catalysts supported on TiO_2 and RE-modified TiO_2 is also barely reported.

Herein, composites of La_2O_3–TiO_2 and CeO_2–TiO_2 were prepared and then Au species were highly dispersed and

[a]*Research Institute of Applied Catalysis, School of Chemical and Environmental Engineering, Shanghai Institute of Technology, Shanghai 201418, P. R. China. E-mail: gzhlu@ecust.edu.cn; Fax: +86-21-60879111*

[b]*Key Laboratory for Advanced Materials and Research Institute of Industrial Catalysis, East China University of Science and Technology, Shanghai 200237, P. R. China. Fax: +86-21-64253824*

supported on the composites. A highly stable Au/TiO_2 catalyst with a long lifetime for CO oxidation was developed by the introduction of RE ions. The role of the RE ions in the Au/La_2O_3–TiO_2 and Au/CeO_2–TiO_2 catalysts was investigated, including the nature of the active sites and the synergism between the Au species and the RE-modified support.

2. Experimental section

2.1. Catalyst preparation

TiO_2 was synthesized by the sol–gel method. 40 vol% tetrabutyl titanate in an anhydrous ethanol solution was poured into a mixed solution (A) of 5 ml water, 10 ml acetic acid, and 25 ml anhydrous ethanol, under vigorous stirring at 40 °C, to obtain an opalescent solution. Subsequently, this solution was continually stirred at 60 °C to form a gel. The gel was dried at 80 °C for 24 h and calcined in air at 550 °C for 6 h. After, a weighed amount of lanthanum nitrate or cerium nitrate was dissolved in solution (A), La_2O_3–TiO_2 or CeO_2–TiO_2 was synthesized by the same steps as described for TiO_2. The RE oxide content was 5 wt%.

A aqueous NaOH solution, 1.0 mol L^{-1}, was slowly poured into a 0.025 mol L^{-1} $HAuCl_4$ solution until the pH = 7.0. Then, TiO_2 (or La_2O_3–TiO_2, CeO_2–TiO_2) particles (>200 mesh) were added to the above-mentioned solution under stirring. This mixed solution was heated to 75 °C and aged for 2 h under continuous stirring, and its pH value was kept at 7.0 by adding NaOH aqueous solution. The solid sample obtained was washed with deionized water several times until the Cl^- ions were not observed in the wash solution, and then it was dried at 80 °C and calcined at 300 °C for 2 h. The obtained catalysts are denoted as Au/TiO_2, Au/La_2O_3–TiO_2 and Au/CeO_2–TiO_2.

2.2. Testing of the catalytic activity

A plug-flow fixed-bed reactor was used to test the activity of the catalysts for CO oxidation. 0.1 g catalyst (60–80 mesh) was used. The reactant gases consisted of 1 vol% CO, 10 vol% O_2, and 89 vol% N_2, and its flow rate was 40 ml min^{-1}. The CO content was analyzed by gas chromatography (GC) equipped with a thermal conductivity detector (TCD).

2.3. Catalyst characterization

XRD patterns of the samples were obtained using a PANalytical X'Pert diffractometer with Ni β-filtered CuKα (λ = 0.15418 nm) radiation at 40 kV and 40 mA. The mean crystallite size of a sample was estimated by the Scherrer equation ($D = K\lambda/\beta \cos\theta$), and the microstrain of a sample was estimated by the equation of $\varepsilon = \beta/4 \text{ tg } \theta$, where K is the constant related to the sample and experimental conditions, λ is the diffraction wavelength, β is the half-high width, and θ is the diffraction angle. The surface areas of the catalysts were measured by N_2 adsorption at −196 °C on a Micromeritics ASAP 2020M + C adsorption apparatus and calculated by the Brunauer–Emmett–Teller (BET) method. Prior to N_2 adsorption, the catalysts were degassed under a vacuum of 10^{-1} Pa for 10 h at 200 °C. The Au content in the catalyst was analyzed on an ICP-AES Philips PV8250 spectrometer. Transmission electron microscopy (TEM) images were obtained on a JEM-2100 electron microscope operated at 200 kV.

The H_2-temperature programmed reduction (H_2-TPR) of the samples was carried out in a quartz microreactor. 0.2 g catalyst (60–80 mesh) was used and pretreated under N_2 (40 ml min^{-1}) at 500 °C for 1 h. Subsequently, the temperature was lowered to room temperature, and the sample was heated in a flowing 10% H_2/N_2 stream (40 ml min^{-1}) up to 620 °C at 15 °C min^{-1}. A quadrupole mass spectrometer (QMS, OmniStar 200) was then used to monitor the desorbed gases.

The *in situ* FT-IR spectra of CO adsorbed on the catalyst were measured on a Nicolet 6700 FT-IR spectrometer equipped with a diffuse reflectance infrared Fourier transform (DRIFT) cell with KBr windows. The sample in the cell was pretreated under N_2 (30 ml min^{-1}) at 300 °C for 2 h, and then the temperature was lowered to room temperature. After the cell was outgassed under vacuum to $<10^{-3}$ Pa, the background was recorded. Followed by introducing CO into the IR cell ($p_{CO} = 8.0 \times 10^3$ Pa), the IR spectrum of CO adsorbed on the catalyst was recorded. The concentration of CO was higher than 99.97%, and it was pretreated by dehydration and deoxygenization before being used. The spectral resolution was 4 cm^{-1} and the number of scans was 32.

3. Results and discussion

3.1. Catalytic activity for CO oxidation

The catalytic activities of Au/TiO_2, Au/La_2O_3–TiO_2 and Au/CeO_2–TiO_2 for CO oxidation are presented in Fig. 1. Among the three catalysts, Au/TiO_2 exhibits the lowest activity with a $T_{50\%}$

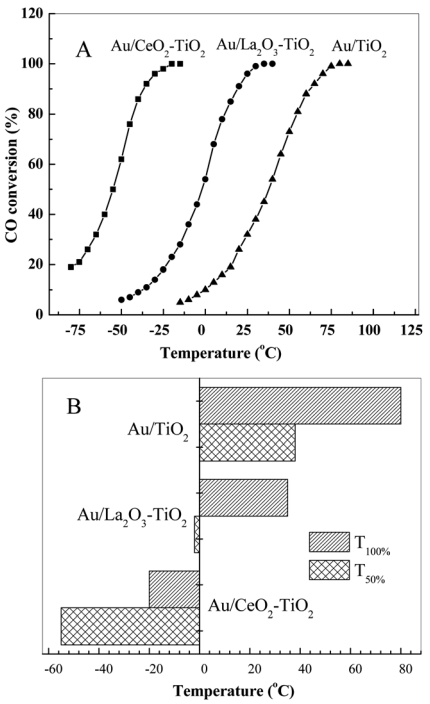

Fig. 1 Catalytic performances of Au/TiO_2, Au/La_2O_3–TiO_2 and Au/CeO_2–TiO_2 for CO oxidation.

(temperature of 50% CO conversion) of 38 °C and $T_{100\%}$ of 80 °C. Au/CeO_2–TiO_2 displays the highest catalytic activity, its $T_{100\%}$ is only −20 °C. The next highest activity is Au/La_2O_3–TiO_2. These results show that CeO_2 and La_2O_3, especially CeO_2, are very effective promoters for the Au/TiO_2 catalyst.

Fig. 2 illustrates the relationship between the catalytic activity and the reaction time of supported Au catalysts for CO oxidation. It can be seen that the catalytic activity of Au/TiO_2 displays a dramatic decrease with reaction time at 60 °C, and decays by 48% after 8 h of reaction. It is interesting to note that the doping of rare earth additives can obviously improve the stability of Au/TiO_2. The Au/CeO_2–TiO_2 catalyst shows the highest stability among the three catalysts, for instance, 100% CO conversion can be maintained after 13 h of reaction at 0 °C, and only decays by 9% after 40 h of reaction.

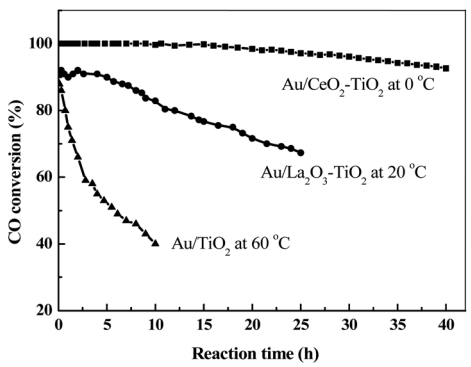

Fig. 2 CO conversion as a function of time on stream over Au/TiO_2 at 60 °C, Au/La_2O_3–TiO_2 at 20 °C and Au/CeO_2–TiO_2 at 0 °C.

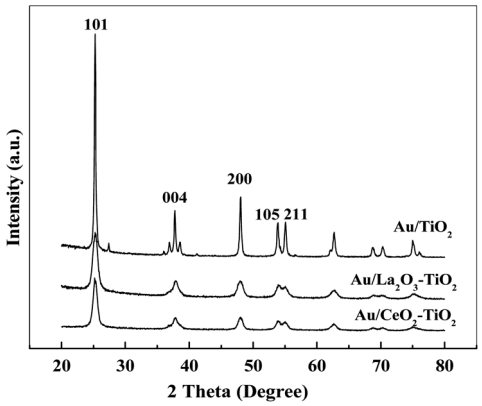

Fig. 3 Powder XRD patterns of Au/TiO_2, Au/La_2O_3–TiO_2 and Au/CeO_2–TiO_2.

3.2. Characterization of the catalysts

The XRD patterns of the catalysts are shown in Fig. 3. The results show that there are TiO_2 diffraction peaks with the anatase-type structure, but no diffraction peaks of gold can be observed. This indicates that the Au particles are highly dispersed on the supports due to the lower content (0.28–0.42 wt%, Table 1). With an addition of La_2O_3 or CeO_2, the diffraction peaks of TiO_2 are obviously broadened, that is, the grain size of TiO_2 becomes small and the microstrain of TiO_2 increases (Table 1). It is conceivable that the formation of Ti–O–Ce (or La) bonds in Ce (La)–TiO_2 can prevent grain growth in TiO_2. In addition, the diffraction peaks of La_2O_3 or CeO_2 are also not observed for Au/La_2O_3–TiO_2 and Au/CeO_2–TiO_2 catalysts, illustrating that La_2O_3 or CeO_2 in the catalysts is highly dispersed.

The TEM images of the catalysts are shown in Fig. 4. It can be seen that the grain sizes of the Au/TiO_2 catalyst are very big and mainly 30–40 nm. For the Au/La_2O_3–TiO_2 and Au/CeO_2–TiO_2 catalysts, the doping of La_2O_3 or CeO_2 restrains the growth of TiO_2 crystallites, and their sizes are mainly 6–10 nm. This is in agreement with the result calculated by the Scherrer equation on the basis of the XRD patterns (Table 1). Meanwhile, the difference in grain size between different supports is also reflected by different specific surfaces areas (Table 1). Gold particles are homogeneously deposited on the supports. Compared with the Au/TiO_2 catalyst, it is obvious that the gold species on the La- or Ce-modified TiO_2 tend to eventually form more ultrafine gold nanoparticles on its surface. This is due to the higher surface area and stronger interactions between the adsorbed gold species and the support. In more detail, on smaller size particles of La_2O_3–TiO_2 or CeO_2–TiO_2 (Fig. 4b and c), there are probably a large number of defects, such as oxygen vacancies, together with steps and adatoms on which gold immobilization could easily take place,[29] which is also in line with the Au loading data (Table 1). Relating the activities of the catalysts with their physicochemical properties, it is suggested that the enhancement of the catalytic activity of Au/La_2O_3–TiO_2 and Au/CeO_2–TiO_2 should be attributed to an increase in the microstrain and Au loading (Table 1), compared with the Au/TiO_2 catalyst.

For the Au/La_2O_3–TiO_2 and Au/CeO_2–TiO_2 catalysts, there is no obvious difference between their physicochemical properties, such as the crystal size, microstrain, Au loading and BET surface area. However, the catalytic activity of Au/CeO_2–TiO_2 is much higher than that of Au/La_2O_3–TiO_2. This phenomenon shows that the differences in the catalyst structure alone are not enough to illustrate the differences in the catalytic activity for CO oxidation. To further investigate the interaction between the gold particles and the corresponding supports, the H_2-TPR technique was employed, and the results are shown in Fig. 5. It can be seen that pure TiO_2 is hardly reduced, and La_2O_3–TiO_2 and CeO_2–TiO_2 have very weak reduction peaks at 275–420 °C and 170–320 °C, respectively.

After loading gold onto the surface of the supports, there are a series of strong peaks at 100–300 °C, which correspond

Table 1 Physicochemical properties of Au catalysts on different supports

Catalyst	Au loading (wt%)	S_{BET} ($m^2\ g^{-1}$)	Crystal size (nm)	Microstrain (%)
Au/TiO_2	0.28	34	33.3	0.25
Au/La_2O_3–TiO_2	0.40	71	8.5	0.94
Au/CeO_2–TiO_2	0.42	65	8.9	0.93

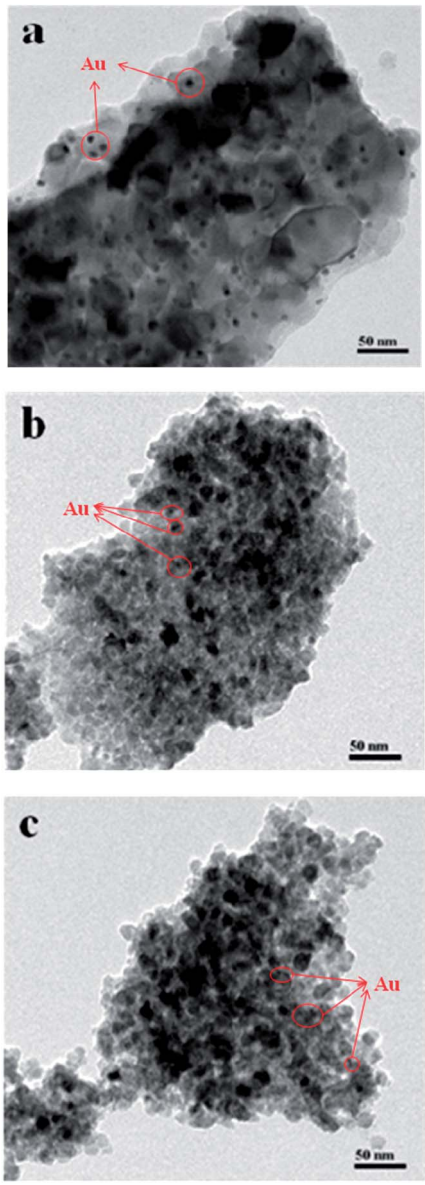

Fig. 4 The TEM images of (a) Au/TiO_2, (b) $Au/La_2O_3–TiO_2$ and (c) $Au/CeO_2–TiO_2$ catalysts.

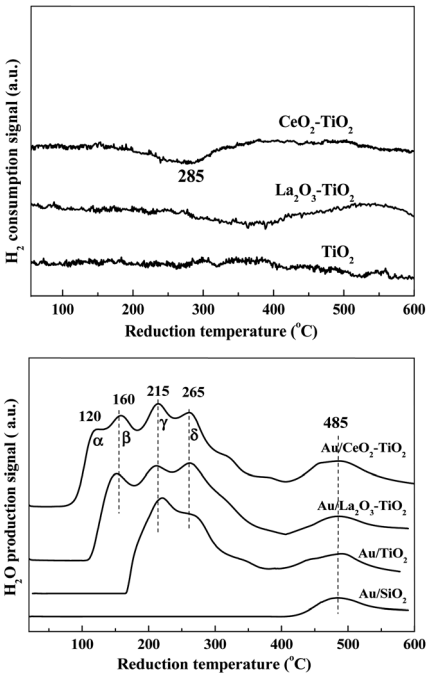

Fig. 5 H_2-TPR-MS curves of the supports and Au catalysts on the different supports.

to the four overlapping reduction peaks (α, β, γ and δ), and there is also a peak at 485 °C. Compared with the reduction peaks of Au supported on quartz, it is suggested that the peak at 485 °C is assigned to the reduction of Au oxide, and the peaks at 100–300 °C seem to be ascribed to the reduction of surface oxygen species of the supports promoted by Au species. Although the reduction peak of Au oxide species is similar for the four samples, the reduction peaks at 100–300 °C are quite different from each other. Only the γ and δ peaks appear in the Au/TiO_2 spectrum, three peaks (β, γ and δ) appear in the $Au/La_2O_3–TiO_2$ spectrum, and the $Au/CeO_2–TiO_2$ spectrum shows four peaks (α, β, γ and δ). According to the results reported by Shapovalov *et al.*,[30] the bond energy of oxygen on the surface of oxides can be weakened by the presence of Au species, indicating that the reduction peaks at 100–300 °C might be attributed to the reduction of surface oxygen species activated by gold species.

Furthermore, the presence of RE oxides improve the properties of the oxygen species on the TiO_2 surface, resulting in the variation of reducibility on the catalyst surface. As CeO_2 possesses a high oxygen storage capacity (OSC) and facile redox cycle of Ce^{3+}/Ce^{4+},[25] the presence of CeO_2 can obviously increase the reactivity of oxygen species on the surface of the catalyst and enhance the mobility of bulk oxygen in the catalyst. Thus, compared with $Au/La_2O_3–TiO_2$, $Au/CeO_2–TiO_2$ may cause more active surface oxygen species by varying Ce^{3+}/Ce^{4+}. This results in the presence of the α peak in the TPR curve. The surface oxygen species on $Au/CeO_2–TiO_2$ occur at a much lower reduction temperature than $Au/La_2O_3–TiO_2$.

To illustrate the redox properties of the catalysts, the repeated TPR for the catalysts is investigated, and the results are presented in Fig. 6. The results show that in the second TPR of all of the samples, no reduction peaks are observed. This is because the surface oxygen species have been exhausted during the first TPR. After the second TPR finished, the samples were cooled in N_2 to room temperature and then exposed to oxygen flow at room temperature for 30 min. The results of the third TPR show that, the reduction peaks at 100–300 °C reappear, but the peak intensities are relatively weak and the reduction peak at 485 °C disappears. These results indicate that the surface oxygen species on the supports can react with hydrogen with help from Au, and the oxygen vacancies left can be restored in oxygen flow at room temperature. Compared with the third TPR curves of Au/TiO_2 and $Au/La_2O_3–TiO_2$, $Au/CeO_2–TiO_2$ still holds the strongest oxygen adsorption ability and possesses the most active oxygen species (represented by the α peak),

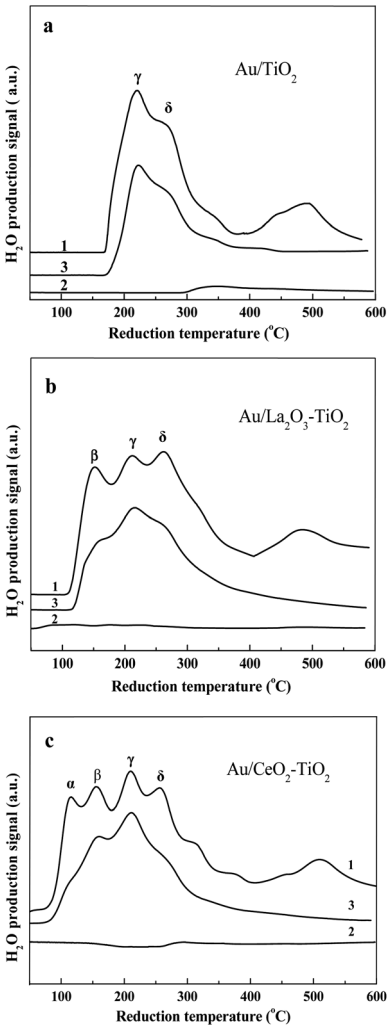

Fig. 6 H_2-TPR-MS profiles of Au/TiO_2, Au/La_2O_3–TiO_2 and Au/CeO_2–TiO_2. (1) First TPR after the catalyst was treated in N_2 at 500 °C for 1 h; (2) the second TPR; (3) the third TPR curve after the sample reduced by the second TPR was exposed to O_2 at room temperature for 0.5 h.

although the α peak in the third TPR curve is smaller than in the first TPR curve.

3.3. CO adsorption on different samples

The CO adsorption on Au/TiO_2, Au/La_2O_3–TiO_2 and Au/CeO_2–TiO_2 was investigated by the *in situ* FT-IR technique, and the results are shown in Fig. 7. The band at 2112 cm^{-1} in the Au/TiO_2 spectrum is ascribed to linear CO species adsorbed on the Au^0 sites,[31,32] and this band in the Au/La_2O_3–TiO_2 and Au/CeO_2–TiO_2 spectra is shifted to 2118 cm^{-1}. Meanwhile, new peaks at 2133 and 2154 cm^{-1} appear in the spectra of the Au/La_2O_3–TiO_2 and Au/CeO_2–TiO_2 catalysts. In general, the blue shift of the carboxylic stretching usually indicates that the Au electrodes shift to a more positive potential. Therefore the bands at 2155–2130 cm^{-1} are ascribed to the feature band of carbonyls on positively charged gold species[33–35] or gold atoms with adsorbed oxygen.[36–38] Compared with the Au/La_2O_3–TiO_2 catalyst, the peak at 2154 cm^{-1} only appears in the Au/CeO_2–TiO_2 spectrum,

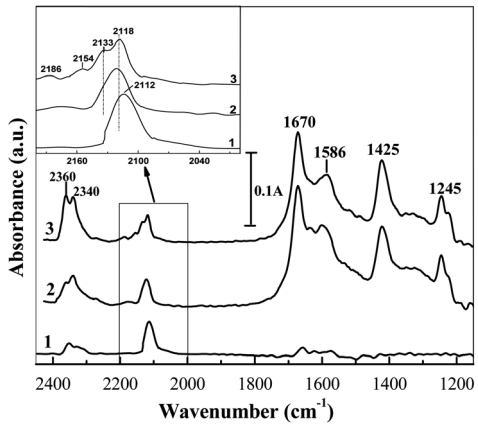

Fig. 7 *In situ* FT-IR absorption spectra of CO (80 mbar) adsorbed on (1) Au/TiO_2, (2) Au/La_2O_3–TiO_2, and (3) Au/CeO_2–TiO_2.

and Au/CeO_2–TiO_2 still has a stronger absorption band at 2133 cm^{-1}. It is conceivable that Au/CeO_2–TiO_2 possesses the more active surface oxygen species interacting with the Au particles, which is consistent with the result of the H_2-TPR. The weak peak at 2186 cm^{-1} in the Au/CeO_2–TiO_2 spectrum is assigned to linear CO species adsorbed on $Ti^{\delta+}$ cations.[39,40]

For Au/La_2O_3–TiO_2 and Au/CeO_2–TiO_2, there are a series of strong bands at 1670, 1586, 1425, 1246 cm^{-1}. These are assigned to the bidentate and monodentate carbonate species adsorbed on the surface,[41,42] and these absorption peaks are not observed in the Au/TiO_2 spectrum.

4. Discussion

4.1. Structure–activity relationship

The results of the XRD, TEM and BET surface area show that the presence of La_2O_3 or CeO_2 can restrain the growth of TiO_2 crystallites, and increase the surface area and microstrain of the TiO_2 support. This promotes an interaction between the Au species and support and causes the presence of Au species of smaller size. As CO oxidation may occur at the interface between the Au particles and TiO_2,[14] the introduction of CeO_2 and La_2O_3 can improve the catalytic activities of the active sites. This results in the high activity of Au/La_2O_3–TiO_2 and Au/CeO_2–TiO_2 for CO oxidation.

4.2. The nature of the active sites

The comparison of the activities of Au/La_2O_3–TiO_2 and Au/CeO_2–TiO_2 with the results of the H_2-TPR and CO adsorption can reveal that in addition to the crystal size and surface area of the support, other factors, such as the redox properties of the sample and the oxidation state of the dispersed Au particles may also influence their catalytic activities. The TPR results (Fig. 5 and 6) show that there are a variety of surface oxygen species on the surface of the TiO_2 support, which are easily reduced with the help of Au species at 100–300 °C. Furthermore, after the reduced catalysts re-adsorb O_2 at room temperature, the reduction peaks at low temperatures can be recovered. This

indicates that the oxygen vacancies formed by the reduction of hydrogen can be restored in an atmosphere containing oxygen. The presence of CeO_2 in the TiO_2 support makes the Au/CeO_2–TiO_2 catalyst possess very strong oxygen adsorption ability and active surface oxygen species. This is a crucial factor with regard to a highly efficient catalyst for low-temperature CO oxidation.[12,15]

In situ FT-IR absorption spectra of CO adsorption (Fig. 7) also reveal that the carboxylic stretching absorption peaks for Au/La_2O_3–TiO_2 and Au/CeO_2–TiO_2 are blue shifted compared to that for Au/TiO_2. The absorption bands of carbonyls on the $(Au_n)^{\delta+}$ sites at 2160–2125 cm^{-1} appear for the Au/La_2O_3–TiO_2 and Au/CeO_2–TiO_2 catalysts, which indicates that the more positively charged Au species exist on these catalysts due to the presence of CeO_2 or La_2O_3. This is because doping with Ce or La is conducive to the formation of $(Au_n)^{\delta+}$ sites with help from surface oxygen species.[43] Among the rare earth oxides, CeO_2 has a unique redox property and high oxygen storage capacity (OSC). It is also the best promoter of oxygen properties (such as mobility and reactivity) for transition metal oxide catalysts. Therefore, more $(Au_n)^{\delta+}$ active sites are formed on the surface of Au/CeO_2–TiO_2 and play a very important role in improving the catalytic activity for low-temperature CO oxidation.

4.3. Reaction mechanism and role of Ce

CO oxidation on a supported gold catalyst occurs on the Au perimeter or Au–support interface.[44] The oxygen atoms from the oxide play a role in the binding of Au particles, and supply oxygen species for the CO oxidation. On the basis of a previous investigation,[45] a schematic of the CO oxidation mechanism is proposed in Fig. 8.

The first step is CO adsorption onto the gold particle, and then the surface carbonyl on the gold particle migrates to the Au–support boundary to transform into an active intermediate. The intermediate is continuously converted into carbonate-like surface species. Once this active intermediate decomposes to the CO_2 product, the active site can be liberated and adsorption of gaseous oxygen can take place. This results in the restoration of the surface oxygen vacancies.

The carbonate species formed on the surface of the catalyst prevents the formation of the active intermediate (or complex). Therefore, it is generally illustrated as the deactivation of Au/TiO_2.[10,11] Based on the results of the H_2-TPR and the *in situ* FT-IR, it is proposed that the Ce-modified Au/TiO_2 possesses a very strong oxygen adsorption ability and active oxygen species at low temperatures. As a result, carbonates are easily decomposed to release CO_2 on the Ce-doped surface and the oxygen vacancies are also readily formed or restored. The high stability of the Au/CeO_2–TiO_2 catalyst is attributed to the oxygen-enriched interface and strong Au–support synergy due to Ce doping. Therefore, the presence of Ce (La) improves the catalytic performance and stability of the Au/TiO_2 catalyst.

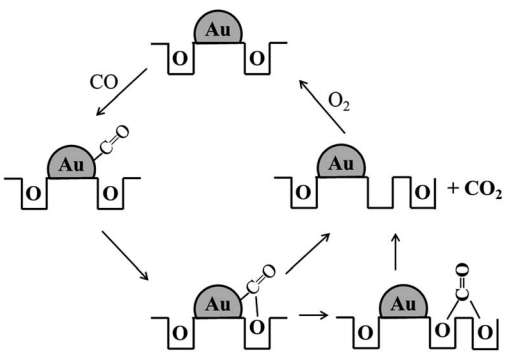

Fig. 8 Mechanism of CO oxidation over a supported Au catalyst.

5. Conclusions

In summary, a highly stable and long lifetime Au/CeO_2–TiO_2 catalyst for CO oxidation was successfully developed and prepared. The doping of cerium or lanthanum obviously improves the catalytic activity for CO oxidation; the effect of CeO_2 on the catalytic activity is much larger than La_2O_3. The results of this research show that doping with an RE oxide can increase the specific surface area, restrain the grain growth, and enhance the microstrain of TiO_2. This results in reinforcing the interaction between the gold species and the support, and the higher dispersion of Au particles on the support.

Doping with ceria or lanthanum oxide improves the synergistic interactions between the support and Au particles, and enhances the reactivity of the surface oxygen species of the catalyst. Because of the redox properties of ceria and more surface oxygen species on CeO_2–TiO_2, more $(Au_n)^{\delta+}$ active sites are formed, resulting in a higher catalytic activity over Au/CeO_2–TiO_2. Moreover, it is clearly revealed that the effortless decomposition of carbonates, and quick recovery of oxygen vacancies caused by the modification of Ce, might be responsible for the high stability of Au/CeO_2–TiO_2.

Acknowledgements

This project was financially supported by the National Natural Science Foundation of China (21273150), the National Basic Research Program of China (2010CB732300, 2013CB933201), the national high technology research and development program of China (2011AA03A406, 2012AA062703), the Fundamental Research Funds for the Central Universities, and the "ShuGuang" Project (10GG23) of Shanghai Municipal Education Commission and Shanghai Education Development Foundation.

Notes and references

1 G. C. Bond and D. T. Thompson, *Catal. Rev. Sci. Eng.*, 1999, **41**, 319.
2 W. G. Menezes, V. Zielasek, K. Thiel, A. Hartwig and M. B. Bäumer, *J. Catal.*, 2013, **299**, 222.
3 M. C. Daniel and D. Astruc, *Chem. Rev.*, 2004, **104**, 293.
4 C. W. Corti, R. J. Holliday and D. T. Thompson, *Appl. Catal., A*, 2005, **291**, 253.
5 D. H. Son, S. M. Hughes, Y. D. Yin and A. P. Alivisatos, *Science*, 2004, **306**, 1009.

6 M. Ojeda, B. Z. Zhan and E. Iglesia, *J. Catal.*, 2012, **285**, 92.
7 G. C. Bond and D. T. Thompsom, *Gold Bull.*, 2000, **33**, 41.
8 W. K. Li, L. N. Chu, X. Q. Gong and G. Z. Lu, *Surf. Sci.*, 2011, **605**, 1369.
9 M. S. Chen and D. W. Goodman, *Science*, 2004, **306**, 252.
10 J. Saavedra, C. Powell, B. Panthi, C. J. Pursell and B. D. Chandler, *J. Catal.*, 2013, **307**, 37.
11 T. A. Ntho, J. A. Anderson and M. S. Scurrell, *J. Catal.*, 2009, **261**, 94.
12 L. M. Liu, B. Mcallister, H. Q. Ye and P. Hu, *J. Am. Chem. Soc.*, 2006, **128**, 4017.
13 A. Chiorino, M. Manzoli, F. Menegazzo, M. Signoretto, F. Vindigni, F. Pinna and F. Boccuzzi, *J. Catal.*, 2009, **262**, 169.
14 M. Comotti, W. C. Li, B. Spliethoff and F. Schüth, *J. Am. Chem. Soc.*, 2006, **128**, 917.
15 M. Kotobuki, R. Leppelt, D. A. Hansgen, D. Widmann and R. J. Behm, *J. Catal.*, 2009, **264**, 67.
16 H. H. Kung, M. C. Kung and C. K. Costello, *J. Catal.*, 2003, **216**, 425.
17 M. Daté, H. Imai, S. Tsubota and M. Haruta, *Catal. Today*, 2007, **122**, 222.
18 M. A. P. Dekkers, M. J. Lippits and B. E. Nieuwenhuys, *Catal. Lett.*, 1998, **56**, 195.
19 F. Boccuzzi, A. Chiorino, M. Manzoli, P. Lu, T. Akita, S. Ichikawa and M. Haruta, *J. Catal.*, 2001, **202**, 256.
20 S. Minicò, S. Scirè, C. Crisafulli and S. Gavagno, *Appl. Catal., B*, 2001, **34**, 277.
21 J. L. Margitfalvi, A. Fási, M. Hegedűs, F. Lónyi, S. Gőbölös and N. Bogdanchikova, *Catal. Today*, 2002, **72**, 157.
22 M. S. Chen and D. W. Goodman, *Catal. Today*, 2006, **111**, 22.
23 M. Haruta, *Gold Bull.*, 2004, **37**, 27.
24 Z. Ma, S. H. Overbury and S. Dai, *J. Mol. Catal. A: Chem.*, 2007, **273**, 186.
25 K. Qian, S. S. Lv, X. Y. Xiao, H. X. Sun, J. Q. Lu, M. F. Luo and W. X. Huang, *J. Mol. Catal. A: Chem.*, 2009, **306**, 40.
26 V. Idakiev, T. Tabakova, K. Tenchev, Z. Y. Yuan, T. Z. Ren and B. L. Su, *Catal. Today*, 2007, **128**, 223.
27 S. Li, H. Q. Zhu, Z. F. Qin, G. F. Wang, Y. G. Zhang, Z. W. Wu, Z. K. Li, G. Chen, W. W. Dong, Z. H. Wu, L. R. Zheng, J. Zhang, T. D. Hu and J. G. Wang, *Appl. Catal., B*, 2014, **144**, 498.
28 N. Sahu, K. M. Parida, A. K. Tripathi and V. S. Kamble, *Appl. Catal., A*, 2011, **399**, 110.
29 N. Lopez, J. K. Nørskov, T. V. W. Janssens, A. Carlsson, A. Puig-Molina, B. S. Calusen and J.-D. Grunwaldt, *J. Catal.*, 2004, **225**, 86.
30 V. Shapovalov and H. Metiu, *J. Catal.*, 2007, **245**, 205.
31 S. Minico, S. Scire, C. Crisafalli, A. M. Visco and S. Galvagno, *Catal. Lett.*, 1997, **47**, 273.
32 F. Boccuzzi, A. Chiorino and M. Manzoli, *Surf. Sci.*, 2000, **454–456**, 942.
33 T. Tabakova, F. Boccuzzi, M. Manzoli, J. W. Sobczak, V. Idakiev and D. Andreeva, *Appl. Catal., B*, 2004, **49**, 73.
34 T. Venkov, K. Fajerwerg, L. Delannoy, H. Klimev, K. Hadjiivanov and C. Louis, *Appl. Catal., A*, 2006, **301**, 106.
35 T. Venkov, H. Klimev, M. A. Centeno, J. A. Odriozola and K. Hadjiivanov, *Catal. Commun.*, 2006, **7**, 308.
36 F. Boccuzzi and A. Chiorino, *J. Phys. Chem. B*, 2000, **104**, 5414.
37 J.-D. Grunwaldt, M. Maciejewski, O. Becker, P. Fabrizioli and A. Baiker, *J. Catal.*, 1999, **186**, 458.
38 D. Guillemot, V. Borokov, V. Kazansky, M. Polisset-Thfoin and J. Fraissard, *J. Chem. Soc., Faraday Trans.*, 1997, **93**, 3587.
39 M. A. Centeno, K. Hadjiivanov, T. Venkov, H. Klimev and J. A. Odriozola, *J. Mol. Catal. A: Chem.*, 2006, **252**, 142.
40 F. Boccuzzi, A. Chiorino, S. Tsubota and M. Haruta, *J. Phys. Chem.*, 1996, **100**, 3625.
41 M. J. Pollard, B. A. Weinstock, T. E. Bitterwolf, P. R. Griffiths, A. P. Newbery and J. P. Paine, *J. Catal.*, 2008, **254**, 218.
42 M. A. Debeila, R. P. K. Wells and J. A. Anderson, *J. Catal.*, 2006, **239**, 162.
43 J. Yu, G. S. Wu, D. S. Mao and G. Z. Lu, *Acta Phys.-Chim. Sin.*, 2008, **24**, 1751.
44 Y. Y. Wu, N. A. Mashayekhi and H. H. Kung, *Catal. Sci. Technol.*, 2013, **3**, 2881.
45 P. Konova, A. Naydenov, C. Venkov, D. Mehandjiev, D. Andreeva and T. Tabakova, *J. Mol. Catal. A: Chem.*, 2004, **213**, 235.